Analytical Chemistry

International Edition: DOI: 10.1002/anie.201605850
German Edition: DOI: 10.1002/ange.201605850

Ultraviolet Photodissociation Induced by Light-Emitting Diodes in a Planar Ion Trap

*Dustin D. Holden, Alexander Makarov, Jae C. Schwartz, James D. Sanders, Eugene Zhuk, and Jennifer S. Brodbelt**

Abstract: *The first application of light-emitting diodes (LEDs) for ultraviolet photodissociation (UVPD) mass spectrometry is reported. LEDs provide a compact, low cost light source and have been incorporated directly into the trapping cell of an Orbitrap mass spectrometer. MS/MS efficiencies of over 50 % were obtained using an extended irradiation period, and UVPD was optimized by modulating the ion trapping parameters to maximize the overlap between the ion cloud and the irradiation volume.*

The development of new ion activation methods, improvement of their efficiencies, and expansion of their range of application are active goals in the field of mass spectrometry. Collision-based methods continue to be the most versatile, robust, and popular activation strategies. Owing to its high energy deposition, which results in the production of rich fragmentation patterns, UVPD has become a powerful alternative activation method for the characterization of small molecules, peptides, nucleic acids, lipids, and proteins.[1–20] The ability to produce intense beams of light is a significant advantage of lasers and makes them a natural fit for UVPD applications, albeit with certain technical hurdles, such as the need for alignment, special optical ports, and in many cases beam collimation and focusing to restrict the laser beam to a prescribed path in the mass spectrometer and minimize damage to other components. The laser beam is normally aligned with the central axis of the ion beam or trapped ions to obtain the highest overlap between ions and photons.[8,12,14–16,18] Moreover, experimental strategies that might benefit from multi-wavelength modes of UVPD require multiple lasers, wavelength-specific dichroics, and precise timing control or, alternatively, a wavelength-tunable optical parametric oscillator (OPO).

The versatile applications of UVPD coupled with the associated challenges of laser-based designs have motivated our interest to implement UVPD in other ways. An alternative source for generating ultraviolet light at lower cost and in a smaller package is light-emitting diodes (LEDs). LED technology has accelerated enormously, in large part due to their widespread adoption as long-lived, highly efficient, and environmentally friendly light sources. Advances in semiconductor optoelectronic materials research have led to the development of LEDs that have extended deeper into the UV range.[21–27] LEDs are commercially available with built-in focusing optics and with output wavelengths between 240 and 950 nm. LEDs also have sufficiently robust performance to be both dimmable and pulsable. Recent studies have shown increases in ultraviolet LED output power[21] and generation of wavelengths as low as 210 nm[22] (although not yet translated into commercial devices).

LEDs have been integrated into analytical applications and spectrometers,[25,28–36] including fluorescence spectroscopy,[28] cost-efficient and compact UV/Vis spectrophotometers,[28–30] and capillary electrophoresis and protein fluorescence detection systems for mass spectrometry.[32–36] Herein, we report the first integration of ultraviolet LEDs with an Orbitrap mass spectrometer to perform UVPD of gas-phase ions.

266 nm UVPD-MS, which is most frequently performed using the fourth harmonic of an Nd:YAG laser, has been used to analyze peptides,[10,17,19,37–39] phosphopeptides,[40,41] and nucleic acids,[42,43] and also to cause selective disulfide bond cleavage.[14,15] UV LEDs, often used for surface disinfection, ozone monitoring, and optical sensing of dyes and inks, are commercially available with emission wavelengths between 255–275 nm. This type of LED was utilized in the present study for application in UVPD. Integrating these LEDs to irradiate a millimeter to sub-millimeter volume occupied by ions proposes a challenge since LEDs are typically designed to provide irradiation over relatively wide angles. Ball lens versions, which were used in this study, confine the beam but are still neither as collimated nor as bright as lasers.

Positioning the LEDs close to the ion cloud to optimize photon/ion overlap was a key design feature for implementing LED-UVPD in an ion trap mass spectrometer. This motivated the design shown in Figure 1, which illustrates the LED higher-energy collisional dissociation (LED-HCD) cell, with a capacity to hold up to 12 LEDs. The standard HCD cell was removed and replaced with this redesigned cell, which includes a custom housing located after the C-trap of an Orbitrap mass spectrometer as shown in the Supporting Information, Figure S1. Further design details are included in the Supporting Information. A single UV LED capable of supplying a high-power, highly focused beam to fully overlap the expected volume of the ion cloud within the ion trap

[*] D. D. Holden, J. D. Sanders, Prof. Dr. J. S. Brodbelt
Department of Chemistry, The University of Texas at Austin
105 E. 24th St, Austin, TX 78712 (USA)
E-mail: jbrodbelt@cm.utexas.edu
Dr. A. Makarov
Thermo Fisher Scientific (Bremen) GmbH
Hanna-Kunath-Strasse 11, 28199 Bremen (Germany)
Dr. J. C. Schwartz, E. Zhuk
Thermo Fisher Scientific Inc.
355 River Oaks Pkwy, San Jose, CA 95134 (USA)
Supporting information and the ORCID identification number(s) for the author(s) of this article can be found under: http://dx.doi.org/10.1002/anie.201605850.

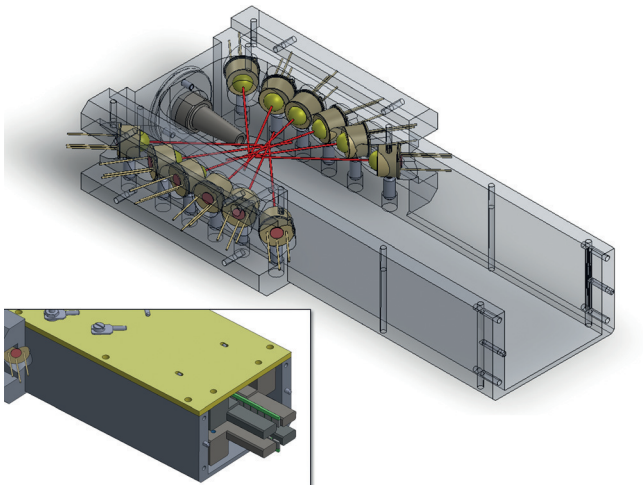

Figure 1. LED-HCD cell with transparent housing and trapping rods removed. Red lines represent the axis of fixed alignment of each LED. The inset shows the cell assembled with planar trapping rods and the cover installed.

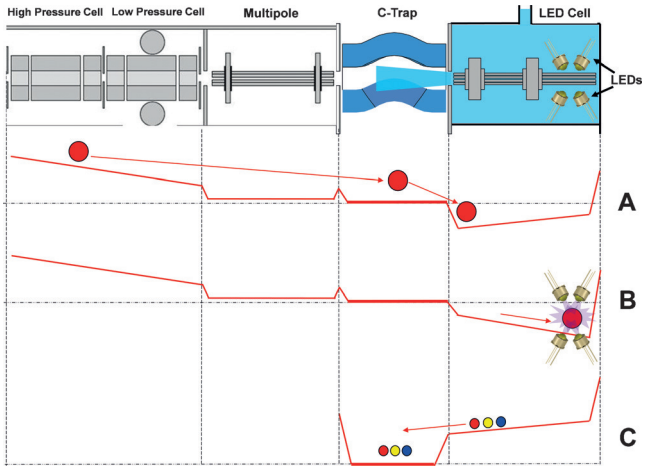

Figure 3. LED-HCD cell with overlays of applied potentials during various experimental steps: A) Ions are transferred to the front of the cell, B) ions are moved to the back of the cell and irradiated, and C) ions are transferred to the C-trap.

(diameter ca. 1 mm) is not yet commercially available, which required the cell design to employ multiple UV LEDs oriented around the ion cloud. As illustrated, the LEDs are positioned towards the back of the LED-HCD cell to allow LED-UVPD to occur only when ions are purposely moved to the back of the cell. This is enabled through the application of an appropriate axial DC gradient by a series of printed circuit boards (PCBs). Figure 2 A is a cross-sectional side view of the

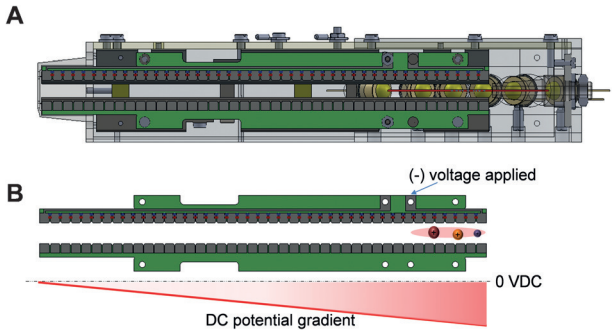

Figure 2. LED-HCD cell: A) Side cross-section view (with trapping rods removed) showing the orientation of the LEDs with axial DC gradient PCBs, B) ion cloud compression after application of a negative voltage to the back electrical contact of the gradient PCBs.

LED-HCD cell illustrating the axial DC PCBs relative to the LEDs. If no voltage is applied to the PCBs, the ions may traverse the entire length of the LED-HCD cell. Once a voltage is applied to one or both ends of the series of PCBs, a DC potential gradient develops, which causes the ions to move in a polarity-dependent direction (Figure 2 B).

A more comprehensive schematic of the mass spectrometer, including the additional dual linear ion trap, multipole, and C-trap components, is shown in Figure 3. (The Orbitrap analyzer used for ion detection is orthogonal to the C-trap and is thus obscured). Precise control of ion position within the LED-HCD cell was performed in three distinct stages: First, the ions were trapped in the front of the cell, during which HCD activation was enabled as desired (Figure 3 A). Second, the ions were transferred from the front of the cell to the back by inverting the slope of the axial DC gradient and trapping them for a period of time depending on the desired LED irradiation time (Figure 3 B). Last, after the LED irradiation period, the resulting fragment ions were transferred to the C-trap prior to Orbitrap detection by again inverting the slope of the DC gradient as shown in Figure 3 C.

After installation of the LEDs and demonstration that ions could be effectively trapped in the LED-HCD cell, an evaluation of LED-UVPD performance was undertaken using a variety of model compounds. The highly conjugated molecule flavin mononucleotide (FMN) has a maximum absorption wavelength (λ_{max}) of 268 nm and a large molar absorption coefficient of 31 620 M^{-1} cm^{-1} in water.[44] Previously, Barran et al. utilized FMN to test the performance of a Q-TOF mass spectrometer equipped with an Nd:YAG laser for 266 nm UVPD.[18] Fragment ions of m/z 243.2, 359.2, and 439.2, which correspond to losses of the side-chain, the phosphate group, and water, respectively, were observed. Additionally, fragments at m/z 257.2 and 286.2 were attributed to the formation of lumiflavin and formyl-lumiflavin species.[18] The LED-HCD cell was fitted with eight LEDs for testing, including two of each LEDs with emission wavelengths of 255, 265, and 275 nm, oriented as shown in the Supporting Information, Figure S1. MS/MS spectra of protonated FMN obtained using the LED-HCD cell are shown in Figure 4. HCD, carried out using a normalized collision energy (NCE) of 16 (14 eV), led to the formation of fragment ions of m/z 243.09, 359.14, and 439.10, all of which were previously observed by Barran et al.[18] By using the ion transfer sequence previously described (Figure 3), protonated FMN ions were trapped and irradiated in the back of the LED-HCD cell for 100 ms to generate the mass spectrum shown in Figure 4 B. Notably, the relative abundance of the ion of m/z 439.10 (water loss) was lower and the abundances

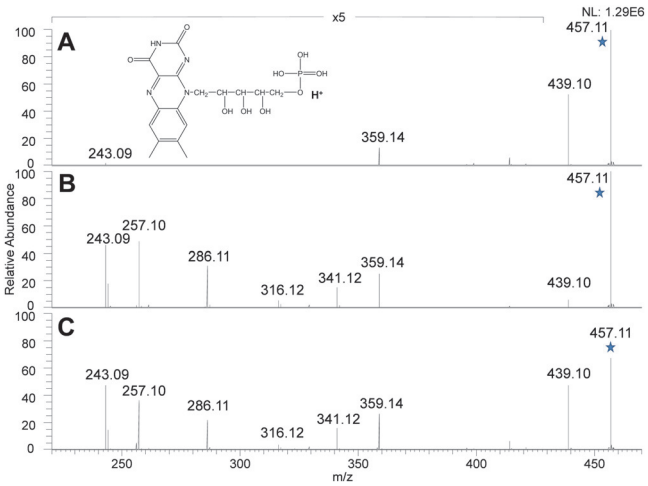

Figure 4. MS/MS spectra of protonated FMN. A) HCD with 16 NCE (0.10 ms), B) LED UVPD with a 100 ms irradiation time, and C) LED UVPD with 16 NCE and 100 ms LED irradiation time. All spectra are shown with similar scaling.

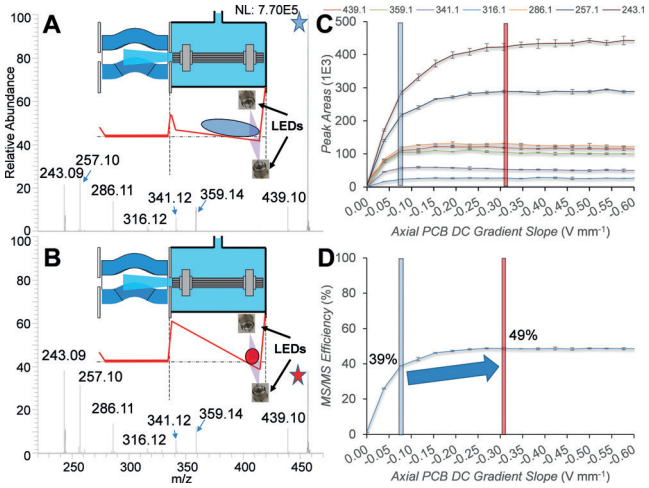

Figure 5. Depiction of ion cloud compression and resulting LED-UVPD mass spectra of protonated FMN obtained with an irradiation period of 500 ms and an adjusted axial DC gradient slope of A) $-0.08\ V\,mm^{-1}$ and B) $-0.31\ V\,mm^{-1}$. C) Fragment ion peak areas as a function of the DC gradient slope and D) MS/MS efficiency as a function of the DC gradient slope for LED-UVPD of protonated FMN. Spectra are shown with similar scaling.

of three key product ions (*m*/*z* 243.09, 257.10, and 286.11) were greater than the distribution observed upon HCD, an outcome that agrees well with the photodissociation observations reported by Barran et al.[18] A hybrid activation method that combined HCD with LED-UVPD (100 ms irradiation time) resulted in the spectrum shown in Figure 4C, thus capitalizing on the ability to augment fragmentation by using complementary activation methods.

An exceptional feature of the axial PCBs is the ability to move ions from one end of the cell to the other as well as compress the ion cloud. As a gauge of the level of control over ion position and UVPD in the LED-HCD cell, the photodissociation of protonated FMN was evaluated based on the position of the ion cloud. Fragmentation only occurred once the ions were moved to the back of the cell during LED irradiation (Supporting Information, Figure S2). The ability to compress the ion cloud in the back of the LED-HCD cell is shown in Figure 5. Figure 5A depicts a shallow DC potential gradient and the resulting LED-UVPD mass spectrum of protonated FMN after a 500 ms irradiation period. Increasing the gradient slope led to the mass spectrum in Figure 5B with a notable increase in UVPD efficiency. The UVPD spectra were monitored while the slope of the DC gradient was varied, generating the graph in Figure 5C, which shows an increase in UVPD, as evidenced by the increasing abundances of fragment ions, until a gradient slope of $-0.31\ V\,mm^{-1}$ is reached. The fragment ions of *m*/*z* 243, 257, and 286 exhibited the most dramatic increase in abundance. Although the fragment ion of *m*/*z* 243 is observed in low abundance during HCD (Figure 4A), its abundance was enhanced during LED-UVPD along with the UVPD specific fragment ions (*m*/*z* 257 and 286). MS/MS efficiencies are plotted in Figure 5D as a function of the DC potential gradient slope, showing a 10% increase in MS/MS efficiency from a slope of -0.08 to $-0.31\ V\,mm^{-1}$. This result suggests that there is an optimal overlap between the trapped ions and the photons when a steeper gradient slope is used to concentrate ions in a defined LED irradiation volume. Reorienting the LED alignment angles and decreasing the ion cloud compression factor to cause the irradiation of a greater portion of the ion cloud is an alternative design concept. This would require higher power output LEDs as well as curtail the capability to restrict irradiation to a particular section of the cell, thus impeding the selection of LED-UVPD versus HCD activation by the user. The results obtained indicate that compressing the ion cloud is indeed beneficial for enhancing ion/photon overlap and increasing the efficiency of LED-UVPD.

After optimization of the DC potential gradient, the MS/MS efficiency was measured as a function of LED irradiation time for protonated FMN (Supporting Information, Figure S3). The MS/MS efficiency reached a maximum of 51% at an irradiation time of 600 ms, including abundances of some low-mass fragment ions (*m*/*z* 172, 186, 214), which increased at longer times (Supporting Information, Figure S3C), suggesting the possibility of secondary fragmentation pathways upon extended LED irradiation. The beam patterns of the LEDs and their impact on LED-UVPD were further examined and are summarized in the Supporting Information, Figure S4.

LED-UVPD was performed on a peptide, doubly protonated angiotensin II (AngII, sequence DRVYIHPF, MW = 1046.2 Da), which resulted in the spectrum shown in the Supporting Information, Figure S5. The only fragment ions observed were those that originated from cleavages in proximity to the Tyr residue (Y), including the a_3 and v_5 backbone ions, loss of the Y side-chain, and an internal ion (VYI) (Supporting Information, Figure S5A). All of the products suggest that Tyr is a key chromophore that modulates the peptide fragmentation upon irradiation using 255–275 nm photons from the LEDs. The MS/MS efficiency as a function of irradiation time is shown as an inset in the Supporting Information, Figure S5A. Even after 2 s of

irradiation, a maximum fragmentation efficiency was not reached. For comparison, the UVPD mass spectrum of AngII (2+) obtained using 2 pulses from a Nd:YAG laser (266 nm, 6 mJ per pulse) is shown in the Supporting Information, Figure S5B. Similar fragments as those produced by LED-UVPD are observed (a_3, v_5, -Y), in addition to other diagnostic a,b,c,y,z sequence ions that are not observed upon LED-UVPD. Backbone cleavages of peptides using 266 nm photons are likely to be multiphoton processes, and thus a high energy Nd:YAG laser is able to access fragmentation pathways not possible for low-power LEDs. Other peptides subjected to LED-UVPD (spectra not shown) were prone to charge reduction and adduction processes owing to reactions with background species at extended irradiation times, which shows that characterization of peptides is not yet a strength of the current array of LEDs. UVPD has also been useful for the analysis of anions in the gas phase, including nucleic acids.[42,43,45] To test the negative mode function of LED-UVPD, the single-stranded oligodeoxynucleotide 5′-GCGCGA-3′ was trapped and irradiated by all eight LEDs for 500 ms. The charge-reduced electron photodetachment (EPD) ion was the dominant product, along with a minor w_5 ion as shown in the Supporting Information, Figure S6A. The isotopic pattern of the EPD product incorporates one less hydrogen atom than a typical doubly deprotonated oligodeoxynucleotide created directly by electrospray ionization (ESI), as shown in the Supporting Information, Figure S6B,C. EPD is commonly observed upon 260–275 nm UVPD of DNA using an Nd:YAG laser,[38,39] and this same process is echoed upon LED-UVPD.

In this first proof-of-principle study, LEDs have been successfully used for UVPD of ions in an HCD cell of an Orbitrap mass spectrometer. MS/MS efficiencies of over 50% were obtained using an extended irradiation period; additionally, it was important to control the ion trapping parameters to maximize the overlap between the ion cloud and the irradiation volume. LED-UVPD of a peptide resulted in the production of some of the same fragment ions observed upon 266 nm UVPD using a Nd:YAG laser, albeit lacking the full array of diagnostic sequence ions. We attribute the less successful performance of LED-UVPD for peptide fragmentation to the low probability of multiphoton absorption using low-power LEDs. LED-UVPD is most effective for ions susceptible to single photon dissociation or electron photodetachment. Even higher UVPD efficiencies are anticipated as LEDs become brighter and LED technology moves into the deeper UV range. A range of wavelengths are currently available in the LED format, and there are compelling opportunities ahead with the possibility of implementing alternating or multiple wavelength strategies. Moreover, the performance metrics of LEDs continue to improve with respect to output power, illumination characteristics, and lifetimes, all factors that signal a promising future for LED-UVPD-MS.

Experimental Section

An Orbitrap Elite mass spectrometer (Thermo Fisher Scientific, Bremen, Germany) fitted with a custom flange and a custom LED-higher-energy collisional dissociation (HCD) cell, as shown in Figure 1, was designed to interface and function with existing hardware and power supplies. Ultraviolet LEDs fitted with fused silica ball lenses and wavelength emissions at 255 nm (UVCLEAN255BL-5), 265 nm (UVCLEAN265BL-5), and 275 nm (UVCLEAN275BL-5) with 3–5 mW power output rating were purchased from Sensor Electronic Technology, Inc. (Columbia, SC). Additional experimental details are given in the Supporting Information.

Acknowledgements

Support from the National Science Foundation (CHE1402753) and the Welch Foundation (F1155) is gratefully acknowledged. We thank Jens Griep-Raming, Scott T. Quarmby, and James M. Hitchcock for fruitful conceptual conversation. We also thank Julia R. Aponte for assistance with DNA sample preparation and analysis.

Keywords: ion traps · light-emitting diodes · mass spectrometry · UV photodissociation

How to cite: *Angew. Chem. Int. Ed.* **2016**, *55*, 12417–12421
Angew. Chem. **2016**, *128*, 12605–12609

[1] N. Webber, Y. He, J. P. Reilly, *J. Am. Soc. Mass Spectrom.* **2014**, *25*, 196–203.
[2] T.-Y. Kim, J. P. Reilly, *J. Am. Soc. Mass Spectrom.* **2009**, *20*, 2334–2341.
[3] Y. M. E. Fung, F. Kjeldsen, O. A. Silivra, T. W. D. Chan, R. A. Zubarev, *Angew. Chem. Int. Ed.* **2005**, *44*, 6399–6403; *Angew. Chem.* **2005**, *117*, 6557–6561.
[4] Y. He, R. Parthasarathi, K. Raghavachari, J. P. Reilly, *J. Am. Soc. Mass Spectrom.* **2012**, *23*, 1182–1190.
[5] D. D. Holden, J. M. Pruet, J. S. Brodbelt, *Int. J. Mass Spectrom.* **2015**, *390*, 81–90.
[6] J. R. Cannon, K. Martinez-Fonts, S. A. Robotham, A. Matouschek, J. S. Brodbelt, *Anal. Chem.* **2015**, *87*, 1812–1820.
[7] M. B. Cammarata, R. Thyer, J. Rosenberg, A. Ellington, J. S. Brodbelt, *J. Am. Chem. Soc.* **2015**, *137*, 9128–9135.
[8] J. B. Shaw, W. Li, D. D. Holden, Y. Zhang, J. Griep-Raming, R. T. Fellers, B. P. Early, P. M. Thomas, N. L. Kelleher, J. S. Brodbelt, *J. Am. Chem. Soc.* **2013**, *135*, 12646–12651.
[9] J. H. Moon, Y. S. Shin, H. J. Cha, M. S. Kim, *Rapid Commun. Mass Spectrom.* **2007**, *21*, 359–368.
[10] C.-K. Lai, D. C. M. Ng, H. F. Pang, J. C. Y. Le Blanc, J. W. Hager, D.-C. Fang, A. S.-C. Cheung, I. K. Chu, *Rapid Commun. Mass Spectrom.* **2013**, *27*, 1119–1127.
[11] J. W. Morgan, D. H. Russell, *J. Am. Soc. Mass Spectrom.* **2006**, *17*, 721–729.
[12] Z. Guan, N. L. Kelleher, P. B. O'Connor, D. J. Aaserud, D. P. Little, F. W. McLafferty, *Int. J. Mass Spectrom. Ion Process.* **1996**, *157–158*, 357–364.
[13] S. H. Yoon, J. H. Moon, M. S. Kim, *J. Mass Spectrom.* **2010**, *45*, 806–814.
[14] P. Wongkongkathep, H. Li, X. Zhang, R. R. Ogorzalek Loo, R. R. Julian, J. A. Loo, *Int. J. Mass Spectrom.* **2015**, *390*, 137–145.
[15] A. Agarwal, J. K. Diedrich, R. R. Julian, *Anal. Chem.* **2011**, *83*, 6455–6458.
[16] M. Girod, Z. Sanader, M. Vojkovic, R. Antoine, L. MacAleese, J. Lemoine, V. Bonacic-Koutecky, P. Dugourd, *J. Am. Soc. Mass Spectrom.* **2015**, *26*, 432–443.

[17] J. Y. Oh, J. H. Moon, M. S. Kim, *Rapid Commun. Mass Spectrom.* **2004**, *18*, 2706 – 2712.
[18] B. Bellina, J. M. Brown, J. Ujma, P. Murray, K. Giles, M. Morris, I. Compagnon, P. E. Barran, *Analyst* **2014**, *139*, 6348 – 6351.
[19] B. Moore, Q. Sun, J. C. Hsu, A. H. Lee, G. C. Yoo, T. Ly, R. R. Julian, *J. Am. Soc. Mass Spectrom.* **2012**, *23*, 460 – 468.
[20] K. L. Fort, A. Dyachenko, C. M. Potel, E. Corradini, F. Marino, A. Barendregt, A. A. Makarov, R. A. Scheltema, A. J. R. Heck, *Anal. Chem.* **2016**, *88*, 2303 – 2310.
[21] D. Y. Kim, J. H. Park, J. W. Lee, S. Hwang, S. J. Oh, J. Kim, C. Sone, E. F. Schubert, J. K. Kim, *Light Sci. Appl.* **2015**, *4*, e263.
[22] Y. Taniyasu, M. Kasu, T. Makimoto, *Nature* **2006**, *441*, 325 – 328.
[23] X. Bai, G. Caputo, Z. Hao, V. T. Freitas, J. Zhang, R. L. Longo, O. L. Malta, R. A. S. Ferreira, N. Pinna, *Nat. Commun.* **2014**, *5*, 5702.
[24] C. Y. Bing, A. A. Mohanan, T. Saha, R. Nagasundara Ramanan, R. Parthiban, N. Ramakrishnan, *Microelectron. Eng.* **2014**, *122*, 9 – 12.
[25] C. Gui, K. Wang, C. Li, X. Dai, D. Cui, *Nanoscale Res. Lett.* **2014**, *9*, 57.
[26] R. M. Jenny, M. N. Jasper, O. D. Simmons, M. Shatalov, J. J. Ducoste, *Water Res.* **2015**, *83*, 310 – 318.
[27] T. Wu, Q. Zha, W. Chen, Z. Xu, T. Wang, X. He, *Atmos. Environ.* **2014**, *95*, 544 – 551.
[28] A. E. Moe, S. Marx, N. Banani, M. Liu, B. Marquardt, D. M. Wilson, *Sens. Actuators B* **2005**, *111 – 112*, 230 – 241.
[29] K. A. Mohammad, A. Zekry, M. Abouelatta, *Int. J. Eng. Technol.* **2015**, *4*, 399.
[30] D. X. Kerola, C. J. Bruegge, H. N. Gross, M. C. Helmlinger, *IEEE Trans. Geosci. Remote Sens.* **2009**, *47*, 1244 – 1255.
[31] P. K. Dasgupta, I.-Y. Eom, K. J. Morris, J. Li, *Anal. Chim. Acta* **2003**, *500*, 337 – 364.
[32] J. D. Russell, M. Scalf, A. J. Book, D. T. Ladror, R. D. Vierstra, L. M. Smith, J. J. Coon, *PLoS ONE* **2013**, *8*, e58157.
[33] J. D. Russell, R. T. Hilger, D. T. Ladror, M. A. Tervo, M. Scalf, M. R. Shortreed, J. J. Coon, L. M. Smith, *Anal. Chem.* **2011**, *83*, 2187 – 2193.
[34] M. O'Toole, D. Diamond, *Sensors* **2008**, *8*, 2453 – 2479.
[35] C. Sluszny, Y. He, E. S. Yeung, *Electrophoresis* **2005**, *26*, 4197 – 4203.
[36] A. Su, *Talanta* **2004**, *64*, 970 – 974.
[37] S. A. Robotham, J. S. Brodbelt, *J. Am. Soc. Mass Spectrom.* **2015**, *26*, 1570 – 1579.
[38] Q. Sun, S. Yin, J. A. Loo, R. R. Julian, *Anal. Chem.* **2010**, *82*, 3826 – 3833.
[39] Y. Tao, N. R. Quebbemann, R. R. Julian, *Anal. Chem.* **2012**, *84*, 6814 – 6820.
[40] S. Park, W.-K. Ahn, S. Lee, S. Y. Han, B. K. Rhee, H. B. Oh, *Rapid Commun. Mass Spectrom.* **2009**, *23*, 3609 – 3620.
[41] J. K. Diedrich, R. R. Julian, *J. Am. Chem. Soc.* **2008**, *130*, 12212 – 12213.
[42] V. Gabelica, F. Rosu, T. Tabarin, C. Kinet, R. Antoine, M. Broyer, E. De Pauw, P. Dugourd, *J. Am. Chem. Soc.* **2007**, *129*, 4706 – 4713.
[43] V. Gabelica, T. Tabarin, R. Antoine, F. Rosu, I. Compagnon, M. Broyer, E. De Pauw, P. Dugourd, *Anal. Chem.* **2006**, *78*, 6564 – 6572.
[44] E. Zondag, J. Posthuma, W. Berends, *Biochim. Biophys. Acta* **1960**, *39*, 178 – 180.
[45] S. I. Smith, J. S. Brodbelt, *Anal. Chem.* **2010**, *82*, 7218 – 7226.

Received: June 17, 2016
Revised: August 2, 2016
Published online: September 8, 2016

